catalysts

MDPI

Article

# Carbon Dioxide Reforming of Methane over Ni Supported $SiO_2$: Influence of the Preparation Method on the Resulting Structural Properties and Catalytic Activity

**Hua-Ping Ren [1], Shao-Peng Tian [1], Si-Yi Ding [1], Gui-Qiu Huang [2], Min Zhu [1], Qiang Ma [1], Wen-Qi Song [1], Yu-Zhen Zhao [1], Zongcheng Miao [1,*] and Wei Wang [3,*]**

1 School of Science, Xijing University, Xi'an 710123, China; renhuaping@xijing.edu.cn (H.-P.R.); tianshaopeng@xijing.edu.cn (S.-P.T.); dingsiyi@xijing.edu.cn (S.-Y.D.); zhumin@xijing.edu.cn (M.Z.); maqiang@xijing.edu.cn (Q.M.); songwenqi@xijing.edu.cn (W.-Q.S.); zhaoyuzhen@xijing.edu.cn (Y.-Z.Z.)

2 School of Petroleum and Chemical Engineering, Beibu Gulf University, Qinzhou 535011, China; huangguiqiu@bbgu.edu.cn

3 College of Chemistry and Chemical Engineering, BaoJi University of Arts and Sciences, Baoji 721013, China

* Correspondence: miaozongcheng@xijing.edu.cn (Z.M.); wang_wei@bjwlxy.cn (W.W.)

Received: 30 June 2020; Accepted: 15 July 2020; Published: 17 July 2020


**Abstract:** Ni-C/$SiO_2$ and Ni-G/$SiO_2$ catalysts were prepared by a complexed-impregnation method using citric acid and glycine as complexing agents, respectively. Ni/$SiO_2$ was also prepared by the conventional incipient impregnation method. All the catalysts were comparatively tested for carbon dioxide reforming of methane (CDR) at P = 1.0 atm, T = 750 °C, $CO_2/CH_4$ = 1.0, and GHSV = 60,000 $mL \cdot g^{-1} \cdot h^{-1}$. The results showed that Ni-C/$SiO_2$ and Ni-G/$SiO_2$ exhibited better CDR performance, especially regarding stability, than Ni/$SiO_2$. The conversions of $CH_4$ and $CO_2$ were kept constant above 82% and 87% after 20 h of reaction over Ni-C/$SiO_2$ and Ni-G/$SiO_2$ while they were decreased from 81% and 88% to 56% and 59%, respectively, over the Ni/$SiO_2$. The characterization results of the catalysts before and after the reaction showed that the particle size and the distribution of Ni, as well as the interactions between Ni and the support were significantly influenced by the preparation method. As a result, an excellent resistance to the coking deposition and the anti-sintering of Ni was obtained over the Ni-C/$SiO_2$ and Ni-G/$SiO_2$, leading to a highly active and stable CDR performance.

**Keywords:** reforming of methane; carbon dioxide; nickel; stability; complexed impregnation

## 1. Introduction

With increasing environmental awareness, the capture and use of $CO_2$ and $CH_4$, which are the two main greenhouse gases, have received increasing attention [1,2]. The carbon dioxide reforming of methane (CDR), which simultaneously converts $CO_2$ and $CH_4$ into syngas, has been extensively reported [3–5]. In addition to the reduction in greenhouse gas emissions, the syngas produced is $H_2/CO \leq 1$ for CDR, which is the raw material for synthesizing high-value chemicals, such as methanol, higher oxygenates, and long-chain hydrocarbons from Fischer-Tropsch (FT) synthesis [6]. More importantly, compared with other $CO_2$ conversion and utilization technologies, CDR can be directly applied to the reforming reaction of $CH_4$ and $CO_2$ in flue gas [7,8]. Therefore, accelerating the industrialization process of the CDR reaction plays an important role in achieving $CO_2$ emission reduction and efficient utilization.

Although precious metal catalysts such as Pt and Rh show excellent catalytic activity and resistance to coking for CDR, the cost of precious metal-based catalysts is too high, which limits their application

as industrial catalysts. Ni-based catalysts have received increasing attention because of their high activity and low cost. However, the problems of the easy sintering and severe coking of Ni-based catalysts for CDR seriously limits their industrial applications [8–10]. Therefore, improving the catalytic performance of Ni-based catalysts for CDR has become an urgent problem.

Comprehensive analysis of the related catalyst research reports shows that there are three main measures for improving the performance of Ni-based catalysts. One method is to change the acidity and alkalinity of the catalyst carriers, such as MgO [11,12], $Al_2O_3$ [12–14], CaO [15–17], and $CeO_2$ [18–20]. The second method is to dope a small amount of a noble metal such as Rh or a transition metal such as Co into a Ni-based catalyst to prepare a bimetallic catalyst [21–23]. The third is to choose different catalyst preparation methods, such as the preparation of Ni-based catalysts with core-shell structures [24–30], the preparation of Ni-based catalysts by plasma technology [10,31,32], and other methods [33,34].

Therefore, this work aimed to develop Ni-based catalysts with high activity and stability for CDR. For this purpose, glycine and citric acid were used as coordination agents, $SiO_2$ was used as the carrier, and nickel nitrate was used as the precursor of Ni. The complexed-impregnation method was used to adjust the size, distribution, and interactions between the carrier and Ni on the Ni-based catalyst. The Ni-based catalysts were subjected to XRD, TEM, and $H_2$-TPR characterization etc., and were tested for CDR at P = 1.0 atm, T = 750 °C, $CH_4/CO_2$ = 1.0, and gas hourly space velocity (GHSV) = 60,000 $mL \cdot g^{-1} \cdot h^{-1}$. These results showed that the particle size and distribution of Ni and the interactions between the support and Ni of the Ni-based catalyst were significant to the CDR performance. Ni-C/$SiO_2$ and Ni-G/$SiO_2$ exhibited better CDR performance because of their smaller Ni particle sizes and stronger interactions between Ni and $SiO_2$, which contributed to these samples achieving the lowest coke deposition and the least sintering of Ni particles. Thus, the complexed-impregnation method is a very promising method for preparing highly efficient CDR catalysts.

## 2. Results and Discussion

### *2.1. Structural Properties of Catalyst*

The XRD characterization of the calcined and reduced Ni-based catalysts, shown in Figure 1, was used to analyze the structural properties. As shown in Figure 1A, a broad diffraction peak at approximately 23° (2θ) was observed, which is the characteristic diffraction peak of amorphous silica species [35]. Moreover, the characteristic diffraction peaks of (111), (200), (220), (311), and (222) of the cubic NiO plane were obtained at 2θ of approximately 37, 43, 63, 75, and 79° on the calcined catalyst [36,37], implying that only cubic NiO was formed on the calcined catalysts. However, the intensity of the NiO diffraction peaks obviously varied for all the catalysts. Ni-C/Q-10 and Ni-G/Q-10 showed weaker diffraction peaks of NiO than Ni/Q-10, and the NiO crystal size was calculated, as shown in Table 1. From the table, Ni/Q-10 exhibited the largest NiO grain size of 16.54 nm, while Ni-C/Q-10 and Ni-G/Q-10 showed smaller NiO particle sizes of 11.58 and 10.01 nm, respectively. This can be explained by the formation of complexes between $Ni^{2+}$ and the complex agents, which prevents the agglomeration of Ni particles [38,39]. The XRD pattern for the reduced catalysts was showed in Figure 1B, in addition to the broad peak at 2θ of 23° for the amorphous silica species, the diffraction peaks at 2θ of 44, 52, and 76° were assigned to the (111), (200), and (220) diffractions of metallic Ni [36,37,40]. The Ni particle size was also calculated and is shown in Table 1. Unexpectedly, the Ni particle sizes were significantly larger than those of the NiO for the corresponding calcined catalysts, implying that the Ni particles were sintered under the reduction conditions. Moreover, Ni particle sizes of approximately 12 nm were obtained for Ni-C/Q-10 and Ni-G/Q-10, which was obviously smaller than that of Ni/$SiO_2$ (25.34 nm), and the dispersion of Ni was calculated, as shown in Table 1 [41]. The dispersion of Ni on Ni-C/Q-10 and Ni-G/Q-10 was larger than that on Ni/Q-10, which is in agreement with the reference reports [40]. These results are consistent with the TEM results

(Figure 2). The distributions of Ni particles obtained for Ni-C/Q-10 and Ni-G/Q-10 were narrower than that for $Ni/SiO_2$, as shown in Figure 2. These results can be ascribed to complexation with the complexing agents (glycine and citric acid) [40,42].

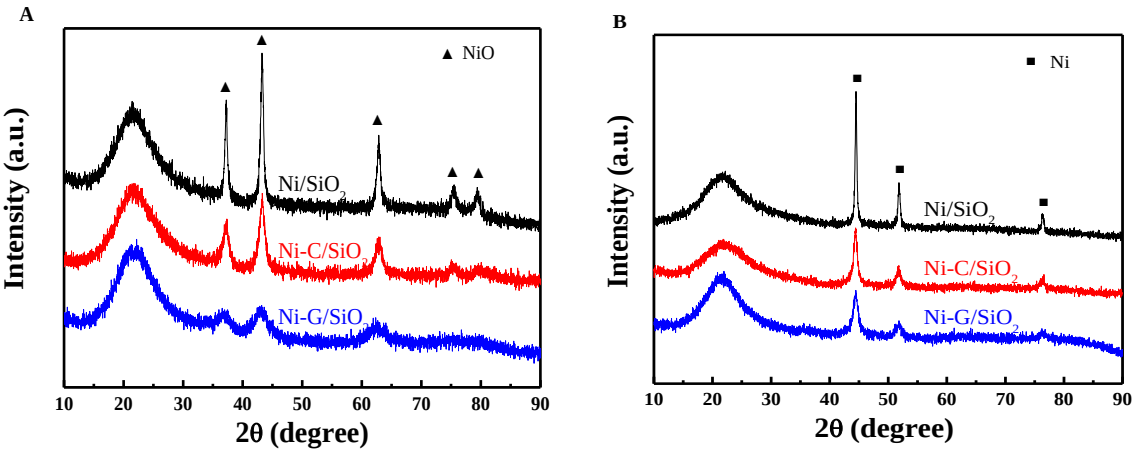


**Figure 1.** XRD pattern for the calcined (**A**) and reduced (**B**) catalysts.

**Table 1.** Summary of the textural and crystal properties of different samples.

| Samples | SBET ($m^2 \cdot g^{-1}$) [a] | Vp ($cm^3 \cdot g^{-1}$) [b] | Dp (nm) [c] | dNiO (nm) [d] | dNi (nm) [e] | dNi (nm) [f] | Dispersion (D%) [g] |
|---|---|---|---|---|---|---|---|
| $SiO_2$ | 271.3 | 0.72 | 11.2 | – | – | – | – |
| $Ni/SiO_2$ | 236.9 | 0.60 | 8.9 | 16.54 | 25.34 | 32.75 | 3.83 |
| $Ni\text{-}C/SiO_2$ | 248.1 | 0.57 | 9.1 | 11.58 | 12.13 | 12.96 | 8.00 |
| $Ni\text{-}G/SiO_2$ | 256.6 | 0.56 | 8.8 | 10.01 | 11.23 | 12.04 | 8.64 |

a: BET surface area; b: total pore volumes calculated by the BJH method with adsorption curves; c: average pore diameter determined by the BJH method; d: calculated by the Scherrer's formula based on the (200) diffraction of the calcined catalyst; e: calculated by the Scherrer's formula based on the (111) diffraction of the reduced catalyst; f: calculated by the Scherrer's formula based on the (111) diffraction of the used catalyst; g: determined by the equation of D% = 97/dNi [41].

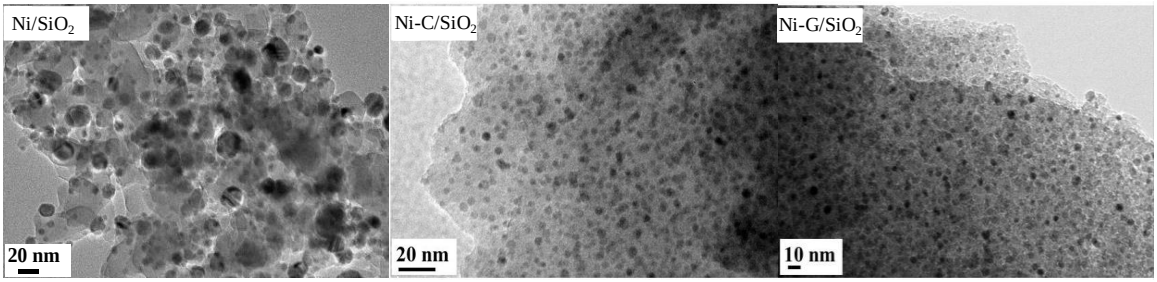


**Figure 2.** TEM images of the reduced catalysts.

### *2.2. Textural Properties of the Catalysts*

The BET surface area, pore volume, and pore diameter of the Ni-based catalysts calculated from the $N_2$ adsorption-desorption isotherms are listed in Table 1. After impregnation with Ni, the BET surface area, pore volume, and pore diameter all obviously decreased. This occurred because the nickel precursor was loaded on the surface of $SiO_2$ and the pore structure, which caused the pores to be blocked, leading to a reduction in the BET specific surface area, pore volume, and pore diameter. However, compared with that of Ni/Q-10, the BET surface areas of Ni-C/Q-10 and Ni-G/Q-10 were larger, implying that the complexing agents formed new pores by decomposing the frame of the complex between $Ni^{2+}$ and the complexing agents [43,44]. Moreover, the pore volume and pore diameter of Ni-C/Q-10 and Ni-G/Q-10 were close to those of Ni/Q-10, implying that the complexing agents were unimportant.

### 2.3. Reduction Behavior of the Catalysts

Figure 3 shows the reduction behavior of the Ni-based catalysts. According to the literature reports, the reduction peak at low temperature (<400 °C) is the reduction of large particles of NiO, and the reduction peak at high temperature can be attributed to the reduction of small particles of NiO and NiO with strong interaction and the support [39,45]. Only one reduction peak at ~370 °C was obtained for Ni/Q-10, while in addition to the reduction peak at approximately 370 °C, a significant reduction peak at approximately 570 °C was obtained for Ni-C/Q-10 and Ni-G/Q-10. This can be explained by the complexation of the complexing agent with metallic Ni, which can significantly reduce the particle size of Ni on the support, resulting in a higher reduction peak [46]. The results are consistent with the previous XRD and TEM results.

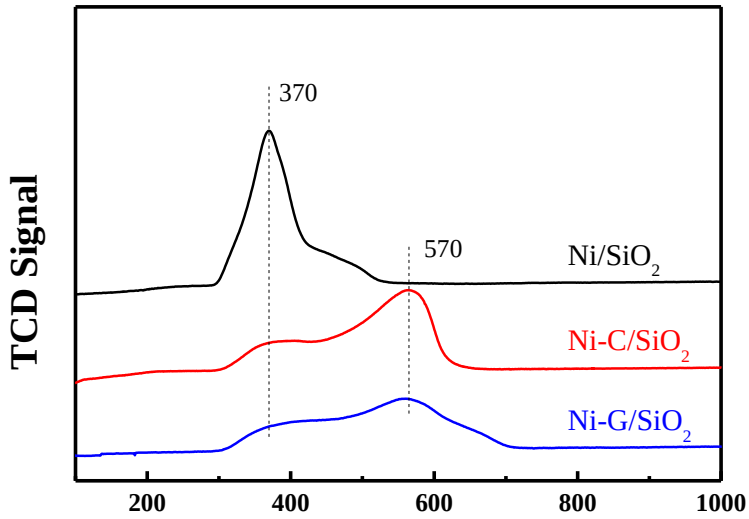


**Figure 3.** $H_2$-TPR patterns for the catalysts.

### 2.4. Catalytic Performance

Figure 4 shows the CDR performance of the Ni-based catalysts under the conditions of P = 1.0 atm, T = 750 °C, $CH_4/CO_2$ = 1.0, and GHSV = 60,000 mL·g$^{-1}$·h$^{-1}$. As shown in Figure 4A, all the Ni-based catalysts showed higher initial CDR activity, which is close to the equilibrium $CH_4$ conversion (83%), and the $CH_4$ conversion at 0.5 h was above 81%. This result is in agreement with the reference reports [47]. However, there were large differences in their stability. The $CH_4$ conversion of Ni/Q-10 decreased rapidly to 56% after 20 h of reaction. Compared with that of Ni/Q-10, the CDR performance of Ni-C/Q-10 and Ni-G/Q-10 was significantly improved, and an unobservable decrease in $CH_4$ was obtained. Therefore, the preparation method has a great influence on the stability of the catalyst for CDR. This can be explained by the smaller size and more uniform distribution of the catalyst prepared by the coordination-impregnation method, which reduces the carbon deposit of the CDR [38–40,42]. This is also completely consistent with the results of the previous discussion.

The $CO_2$ conversion, $H_2/CO$ and $H_2$ yield over all the catalysts exhibited a similar trend as the $CH_4$ conversion (Figure 4B–D). When the conversions of $CH_4$ and $CO_2$ (Figure 4A,B) were carefully compared, all the catalysts showed the higher $CO_2$ conversion than corresponding to $CH_4$ conversion. This can be ascribed to the reverse water gas shift reaction, which is also explained the lower $H_2/CO$ than the equilibrium value shown in Figure 4C. Moreover, a higher $H_2$ yield was obtained over the Ni-C/Q-10 and Ni-G/Q-10 shown in Figure 4D.

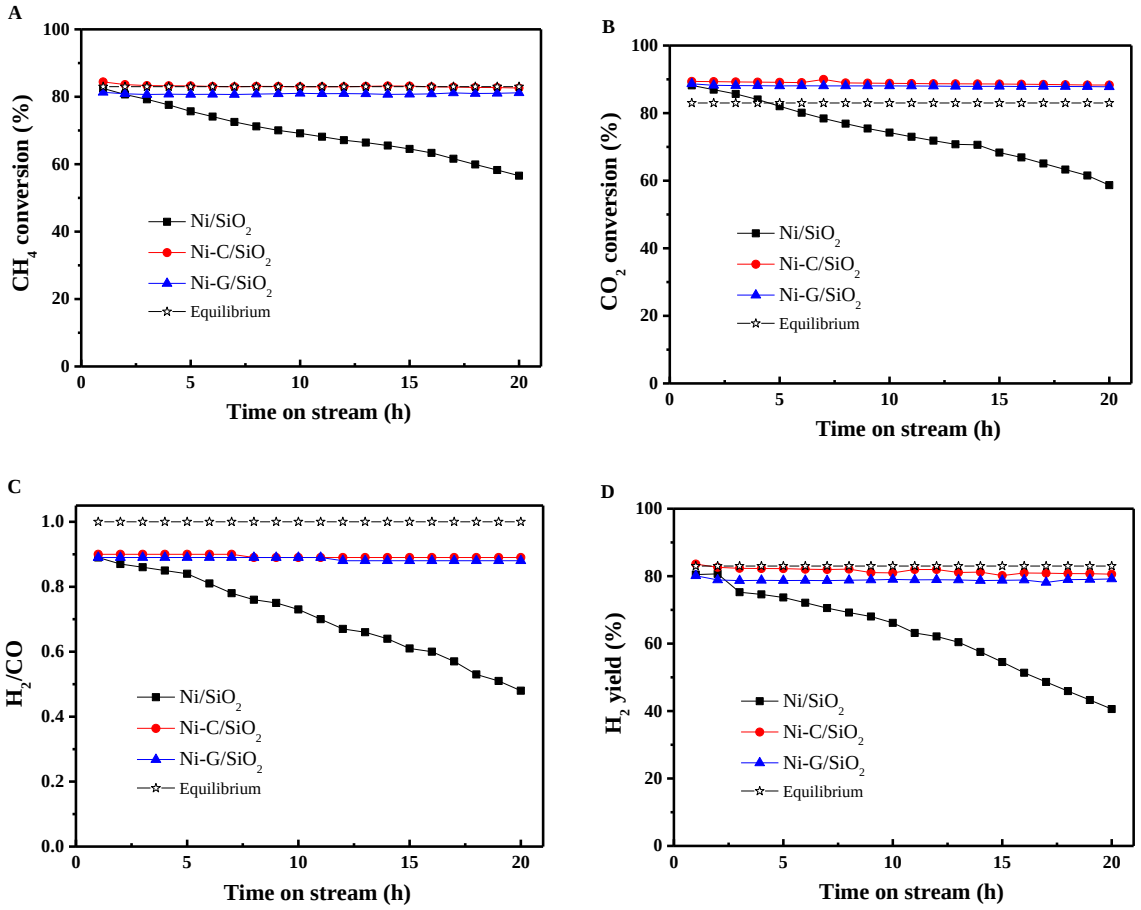


**Figure 4.** Time-on-stream $CH_4$ conversion (**A**), $CO_2$ conversion (**B**), $H_2$/CO (**C**), and $H_2$ yield (**D**) over catalysts under the conditions of P = 1.0 atm, T = 750 °C, $CH_4/CO_2$ = 1.0, and GHSV = 60,000 mL·$g^{-1}$·$h^{-1}$.

## 2.5. Characterization of Used Catalysts

The used catalysts after CDR for TOS = 20 h were subjected to XRD characterization, and the results are shown in Figure 5. Compared with the reduced catalysts (Figure 1), except for the clear shoulder peak at 2θ of approximately 26° for the used Ni/Q-10, similar diffraction peaks were obtained for the used catalysts, implying that they had the same Ni crystal structure after CDR. The diffraction peak at 2θ of approximately 26° was a diffraction peak of graphitic carbon, suggesting that less coke was deposited on Ni-C/Q-10 and Ni-G/Q-10 than on Ni/Q-10, which was attributed to the smaller Ni particle size [8,37]. When the intensities of the Ni diffraction peaks were carefully compared, the peak intensities of the used catalysts were greater than those of the corresponding reduced catalysts, implying Ni sintering after CDR, which agrees with previous reports [37,39]. To clearly express the degree of Ni sintering, the Ni crystal sizes of the used catalyst were calculated and are listed in Table 1. From Table 1, the Ni crystal sizes of the used Ni/Q-10 significantly increased from 25.34 nm to 32.75 nm, while the used Ni-C/Q-10 and Ni-G/Q-10 displayed slight increases, suggesting superior anti-sintering on Ni-C/Q-10 and Ni-G/Q-10. These results are also consistent with the results of a previous report stating that good CDR performance was achieved with catalysts with superior anti-sintering characteristics [37,39,48], which is also supported by the results of TPR (Figure 3), showing a stronger interaction between the Ni and supports [37,39,45,49].

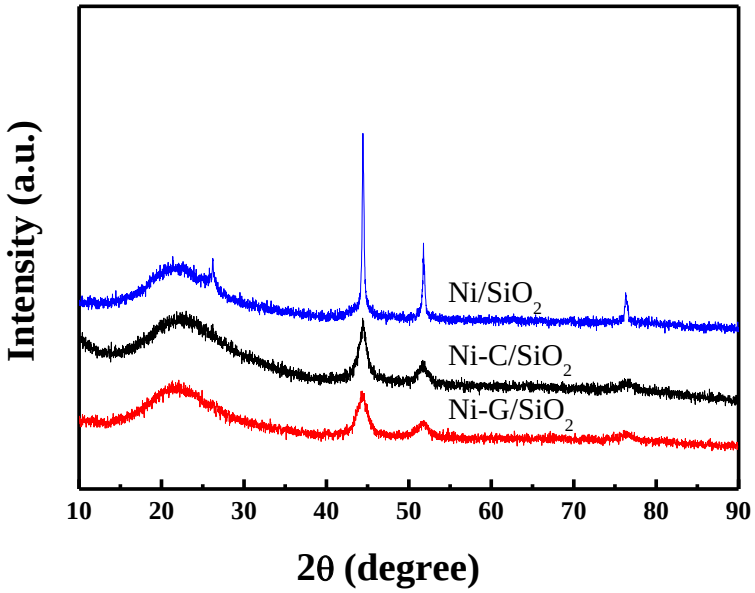


**Figure 5.** XRD pattern for the used catalysts after CDR under the conditions of P = 1.0 atm, T = 750 °C, $CH_4/CO_2$ = 1.0, GHSV = 60,000 mL·$g^{-1}$·$h^{-1}$, and TOS = 20 h.

Moreover, the used catalysts after the CDR reaction were characterized by TG, as shown in Figure 6, to confirm the coke deposition. An observable weight increase occurred at temperatures from approximately 200 °C to 400 °C for all the used catalysts due to the oxidation of Ni to NiO [50], while the weight loss starting from 400 °C was assigned to the gasification of the coke deposited after the CDR reaction. As shown in Figure 6, a slight weight loss about ~1.4–1.7% was obtained for the used Ni-C/Q-10 and Ni-G/Q-10 after 20 h CDR testing, and it was significantly lower than that of the used Ni/Q-10 (3.1%), which is significantly lower than the weight loss of the reference reports [51,52]. These results showed that the coke deposition was significantly reduced by adding complexing agent, which was attributed to its smaller Ni particle sizes (Figure 2 and Table 1) leading to a high stability of CDR (Figure 4).

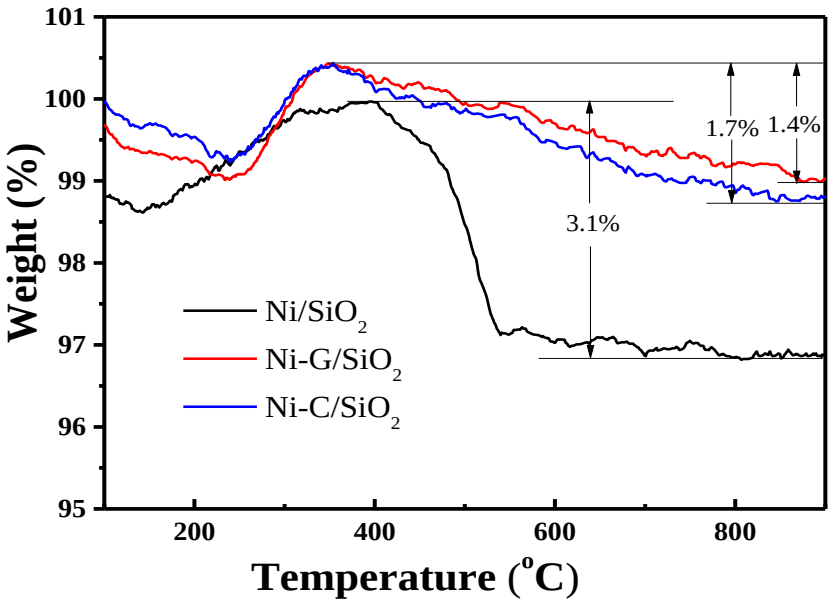


**Figure 6.** TGA curves for the used catalysts after CDR under the conditions of P = 1.0 atm, T = 750 °C, $CH_4/CO_2$ = 1.0, GHSV = 60,000 mL·$g^{-1}$·$h^{-1}$, and TOS = 20 h.

## 3. Materials and Methods

### *3.1. Preparation of Catalysts*

The Ni-supported $SiO_2$ catalysts were prepared by the complexed-impregnation method. Using citric acid (C) and glycine (G) as the complexing agents, commercial $SiO_2$ (Q-10 was purchased from Fujisilicia) was used as the support, and $Ni(NO_3)_2{\cdot}6H_2O$ was used as the precursor of Ni. The nickel content in the catalyst was set to 10 wt.%. Before the impregnation, Q-10 was calcined at 750 °C for 4 h. The $Ni(NO_3)_2{\cdot}6H_2O$ and complexing agent were dissolved in distilled water containing the same volume of Q-10. The molar ratio of the complexing agent to Ni was 0.5. Then, the Q-10 was added to the mixed aqueous solution, and it was continuously oscillated for 30 min until evenly mixed. After the sample was stored at room temperature overnight, it was dried at 80 °C for 12 h and calcined at 500 °C for 4 h. The catalysts were designated Ni-x/Q-10, where x is the complexing agent used. For comparison, Ni/Q-10 was prepared by the same procedure with the same preparation parameters but without the addition of a complexing agent.

### *3.2. Characterization Techniques Used on the Catalysts*

XRD was performed on the samples by an X-ray powder diffractometer (Bruker, Germany, D8 Advance) with Cu Kα radiation (40 kV, 40 mA). The grain sizes of the Ni and NiO were determined by the Scherrer equation based on the (111) and (200) planes, respectively.

The textural properties were measured by a BelSorp-Max physisorption analyzer under liquid nitrogen temperature. The sample was pretreated under vacuum ($10^{-2}$ kPa) at 300 °C for 10 h. The specific surface area of the sample was calculated by the BET method, and the pore volume was tested from the nitrogen adsorption data at the relative pressure ($P/P_0$) = 0.99.

The $H_2$-TPR was tested on a Micromeritics Autochem 2920 instrument. Before testing, the sample was purged with argon (30 mL·min$^{-1}$) at 300 °C for 1 h. The carrier gas was 10% $H_2$/Ar (30 mL·min$^{-1}$).

TEM images were taken on a JEOL JEM-2100 transmission electron microscope. The sample was dispersed in an ethanol solution by ultrasonic sonication for 2 min, dropped on copper grids and dried in air.

The coke deposition of the used catalyst was measured using a Q1000DSC+LNCS+FACS Q600SDT type thermogravimetry-differential thermal analyzer under air atmosphere with a total flow of 100 mL·min$^{-1}$.

### *3.3. Activity Evaluation of the Catalysts*

The CDR was carried out in a fixed bed reactor with a quartz reaction tube (the inner diameter was 8 mm). Then, 0.10 g catalyst (40–60 mesh) was loaded and reduced by 50 mL·min$^{-1}$ 10% $H_2/N_2$, and the temperature was raised to 700 °C for 150 min. After the reduction, it was purged with 40 mL·min$^{-1}$ $N_2$ for 30 min, the temperature was raised to 750 °C, and the flow was switched to the feed gas ($CH_4/CO_2$ = 1.0). The CDR reaction was performed under the conditions of T = 750 °C, P = 1.0 atm, and gas hourly space velocity (GHSV) = 60,000 mL·g$^{-1}$·h$^{-1}$. The product gases, which were condensed in an ice water bath to remove the water, were separated by Molecular Sieve 5A and Porapak Q capillary columns and analyzed by online gas chromatography (GC9720II, Zhejiang Fuli chromatographic analysis Co., Ltd., Zhejiang, China).

## 4. Conclusions

Using citric acid and glycine as complexing agents, Ni-C/$SiO_2$ and Ni-G/$SiO_2$ catalysts were prepared by the complexing-impregnation method. Compared with Ni/$SiO_2$ prepared with the traditional incipient impregnation method, Ni-C/$SiO_2$ and Ni-G/$SiO_2$ show smaller particle sizes and better dispersion of Ni and stronger interactions between Ni and the support $SiO_2$. The CDR performance of the Ni-based catalysts was comparatively studied. Both the catalyst preparation of the coordination-impregnation method and the traditional incipient impregnation method showed

high activity, but the stability was significantly different. More importantly, Ni-C/$SiO_2$ and Ni-G/$SiO_2$ exhibited higher stability, and the $CH_4$ conversion was maintained after 20 h. Combining the results of characterization and CDR, smaller Ni particles and stronger interaction between Ni and the support $SiO_2$ of the Ni-based catalysts are beneficial for suppressing the formation of carbon deposits and Ni sintering at high temperature, resulting in better CDR performance.

**Author Contributions:** H.-P.R. conceived and designed the experiment; Q.M., W.-Q.S., and M.Z. performed the experiments; S.-P.T. and S.-Y.D. analyzed the data; G.-Q.H. and Y.-Z.Z. contributed reagents/materials/analysis; H.-P.R., W.W., and Z.M. wrote the paper. All authors have read and agreed to the published version of the manuscript.

**Funding:** This research was funded by National Natural Science Foundation of China (21908182, 21706218 and 21901214), the Natural Science Foundation of Shaanxi Province (2019JQ-920, 2020JM-643), the Special Scientific Research Project of Shaanxi Education Department (18JK1194), and the Science Research Foundation of Xijing University (XJ17T01, XJ18T03).

**Conflicts of Interest:** The authors declare no conflict of interest.

## References

1. Silva, C.G.; Passos, F.B.; Silva, V.T. Influence of the support on the activity of a supported nickel-promoted molybdenum carbide catalyst for dry reforming of methane. *J. Catal.* **2019**, *375*, 507–518. [CrossRef]
2. Wang, F.; Han, B.; Zhang, L.; Xu, L.; Yu, H.; Shi, W. $CO_2$ reforming with methane over small-sized Ni@$SiO_2$ catalysts with unique features of sintering-free and low carbon. *Appl. Catal. B Environ.* **2018**, *235*, 26–35. [CrossRef]
3. Xie, T.; Shi, L.; Zhang, J.; Zhang, D. Immobilizing Ni nanoparticles to mesoporous silica with size and location control via a polyol-assisted route for coking- and sintering-resistant dry reforming of methane. *Chem. Commun.* **2014**, *50*, 7250–7253. [CrossRef]
4. Yang, W.; Liu, H.; Li, Y.; Wu, H.; He, D. $CO_2$ reforming of methane to syngas over highly-stable Ni/SBA-15 catalysts prepared by P123-assisted method. *Int. J. Hydrog. Energy* **2016**, *41*, 1513–1523. [CrossRef]
5. Li, X.; Li, D.; Tian, H.; Zeng, L.; Zhao, Z.-J.; Gong, J. Dry reforming of methane over Ni/$La_2O_3$ nanorod catalysts with stabilized Ni nanoparticles. *Appl. Catal. B Environ.* **2017**, *202*, 683–694. [CrossRef]
6. Kumar, N.; Roy, A.; Wang, Z.; Abbate, E.M.; Haynes, D.; Shekhawat, D.; Spivey, J.J. Bi-reforming of methane on Ni-based pyrochlore catalyst. *Appl. Catal. A Gen.* **2016**, *517*, 211–216. [CrossRef]
7. Centi, G.; Quadrelli, E.A.; Perathoner, S. Catalysis for $CO_2$ conversion: A key technology for rapid introduction of renewable energy in the value chain of chemical industries. *Energy Environ. Sci.* **2013**, *6*, 1711–1731. [CrossRef]
8. Kawi, S.; Kathiraser, Y.; Ni, J.; Oemar, U.; Li, Z.; Saw, E.T. Progress in synthesis of highly active and stable nickel-based catalysts for carbon dioxide reforming of methane. *ChemSusChem* **2015**, *8*, 3556–3575. [CrossRef]
9. Li, S.; Gong, J. Strategies for improving the performance and stability of Ni-based catalysts for reforming reactions. *Chem. Soc. Rev.* **2014**, *43*, 7245–7256. [CrossRef]
10. Liu, C.-J.; Ye, J.; Jiang, J.; Pan, Y. Progresses in the preparation of coke resistant Ni-based catalyst for steam and $CO_2$ reforming of methane. *ChemCatChem* **2011**, *3*, 529–541. [CrossRef]
11. García, V.; Fernández, J.J.; Ruíz, W.; Mondragón, F.; Moreno, A. Effect of MgO addition on the basicity of Ni/$ZrO_2$ and on its catalytic activity in carbon dioxide reforming of methane. *Catal. Commun.* **2009**, *11*, 240–246. [CrossRef]
12. Pizzolitto, C.; Pupulin, E.; Menegazzo, F.; Ghedini, E.; Michele, A.D.; Mattarelli, M.; Cruciani, G.; Signoretto, M. Nickel based catalysts for methane dry reforming: Effect of supports on catalytic activity and stability. *Int. J. Hydrog. Energy* **2019**, *44*, 28065–28076. [CrossRef]
13. Xu, Y.; Du, X.; Li, J.; Wang, P.; Zhu, J.; Ge, F.; Zhou, J.; Song, M.; Zhu, W. A comparison of $Al_2O_3$ and $SiO_2$ supported Ni-based catalysts in their performance for the dry reforming of methane. *J. Fuel Chem. Technol.* **2019**, *47*, 199–208. [CrossRef]
14. Charisiou, N.D.; Tzounis, L.; Sebastian, V.; Hinder, S.J.; Baker, M.A.; Polychronopoulou, K.; Goula, M.A. Investigating the correlation between deactivation and the carbon deposited on the surface of Ni/$Al_2O_3$ and Ni/$La_2O_3$-$Al_2O_3$ catalysts during the biogas reforming reaction. *Appl. Surf. Sci.* **2019**, *474*, 42–56. [CrossRef]

15. Sun, Y.; Zhang, G.; Liu, J.; Xu, Y.; Lv, Y. Production of syngas via $CO_2$ methane reforming process: Effect of cerium and calcium promoters on the performance of Ni-MSC catalysts. *Int. J. Hydrog. Energy* **2020**, *45*, 640–649. [CrossRef]
16. Shi, C.; Zhang, P. Effect of a second metal (Y, K, Ca, Mn or Cu) addition on the carbon dioxide reforming of methane over nanostructured palladium catalysts. *Appl. Catal. B Environ.* **2012**, *115*, 190–200. [CrossRef]
17. Taherian, Z.; Gharahshiran, V.S.; Khataee, A.; Meshkani, F.; Orooji, Y. Comparative study of modified Ni catalysts over mesoporous CaO-$Al_2O_3$ support for $CO_2$/methane reforming. *Catal. Commun.* **2020**, *145*, 106100. [CrossRef]
18. Charisiou, N.D.; Siakavelas, G.; Papageridis, K.N.; Baklavaridis, A.; Tzounis, L.; Avraam, D.G.; Goula, M.A. Syngas production via the biogas dry reforming reaction over nickel supported on modified with $CeO_2$ and/or $La_2O_3$ alumina catalysts. *J. Nat. Gas Sci. Eng.* **2016**, *31*, 164–183. [CrossRef]
19. Pino, L.; Italiano, C.; Vita, A.; Laganà, M.; Recupero, V. $Ce_{0.70}La_{0.20}Ni_{0.10}O_2$-δ catalyst for methane dry reforming: Influence of reduction temperature on the catalytic activity and stability. *Appl. Catal. B Environ.* **2017**, *218*, 779–792. [CrossRef]
20. Charisiou, N.D.; Siakavelas, G.; Tzounis, L.; Sebastian, V.; Monzon, A.; Baker, M.A.; Hinder, S.J.; Polychronopoulou, K.; Yentekakis, I.V.; Goula, M.A. An in depth investigation of deactivation through carbon formation during the biogas dry reforming reaction for Ni supported on modified with $CeO_2$ and $La_2O_3$ zirconia catalysts. *Int. J. Hydrog. Energy* **2018**, *43*, 18955–18976. [CrossRef]
21. Álvarez, A.; Bobadilla, M.L.F.; Garcilaso, V.; Centeno, M.A.; Odriozola, J.A. $CO_2$ reforming of methane over Ni-Ru supported catalysts: On the nature of active sites by operando DRIFTS study. *J. $CO_2$ Util.* **2018**, *24*, 509–515. [CrossRef]
22. Turap, Y.; Wang, I.; Fu, T.; Wu, Y.; Wang, Y.; Wang, W. Co-Ni alloy supported on $CeO_2$ as a bimetallic catalyst for dry reforming of methane. *Int. J. Hydrog. Energy* **2020**, *45*, 6538–6548. [CrossRef]
23. Andraos, S.; Abbas-Ghaleb, R.; Chlala, D.; Vita, A.; Italiano, C.; Laganà, M.; Pino, L.; Nakhl, M.; Specchia, S. Production of hydrogen by methane dry reforming over ruthenium-nickel based catalysts deposited on $Al_2O_3$, $MgAl_2O_4$, and YSZ. *Int. J. Hydrog. Energy* **2019**, *44*, 25706–25716. [CrossRef]
24. Li, Z.; Mo, L.; Kathiraser, Y.; Kawi, S. Yolk-satellite-shell structured Ni-Yolk@Ni@$SiO_2$ nanocomposite: Superb catalyst toward methane $CO_2$ reforming reaction. *ACS Catal.* **2014**, *4*, 1526–1536. [CrossRef]
25. Zhang, J.; Li, F. Coke-resistant Ni@$SiO_2$ catalyst for dry reforming of methane. *Appl. Catal. B Environ.* **2015**, *176*, 513–521. [CrossRef]
26. Zhang, L.; Wang, F.; Zhu, J.; Han, B.; Fan, W.; Zhao, L.; Cai, W.; Li, Z.; Xu, L.; Yu, H.; et al. $CO_2$ reforming with methane reaction over Ni@$SiO_2$ catalysts coupled by size effect and metal-support interaction. *Fuel* **2019**, *256*, 115954. [CrossRef]
27. Wang, N.; Shen, K.; Huang, L.; Yu, X.; Qian, W.; Chu, W. Facile route for synthesizing ordered mesoporous Ni-Ce-Al oxide materials and their catalytic performance for methane dry reforming to hydrogen and syngas. *ACS Catal.* **2013**, *3*, 1638–1651. [CrossRef]
28. Li, Z.; Jiang, B.; Wang, Z.; Kawi, S. High carbon resistant Ni@Ni phyllosilicate@$SiO_2$ core shell hollow sphere catalysts for low temperature $CH_4$ dry reforming. *J. $CO_2$ Util.* **2018**, *27*, 238–246. [CrossRef]
29. Wang, C.; Jie, X.; Qiu, Y.; Zhao, Y.; Al-Megren, H.A.; Alshihri, S.; Edwards, P.P.; Xiao, T. The importance of inner cavity space within Ni@$SiO_2$ nano-capsule catalysts for excellent coking resistance in the high-space-velocity dry reforming of methane. *Appl. Catal. B Environ.* **2019**, *259*, 118019. [CrossRef]
30. Niu, J.; Ran, J.; Chen, D. Understanding the mechanism of $CO_2$ reforming of methane to syngas on Ni@Pt surface compared with Ni(111) and Pt(111). *Appl. Surf. Scie.* **2020**, *513*, 145840. [CrossRef]
31. Yan, X.; Liu, Y.; Zhao, B.; Wang, Z.; Wang, Y.; Liu, C.-J. Methanation over Ni/$SiO_2$: Effect of the catalyst preparation methodologies. *Int. J. Hydrog. Energy* **2013**, *38*, 2283–2291. [CrossRef]
32. Yan, X.; Hu, T.; Liu, P.; Li, S.; Zhao, B.; Zhang, Q.; Jiao, W.; Chen, S.; Wang, P.; Lu, J.; et al. Highly efficient and stable Ni/$CeO_2$-$SiO_2$ catalyst for dry reforming of methane: Effect of interfacial structure of Ni/$CeO_2$ on $SiO_2$. *Appl. Catal. B Environ.* **2019**, *246*, 221–231. [CrossRef]
33. Palma, V.; Barba, D.; Cortese, M.; Martino, M.; Renda, S.; Meloni, E. Microwaves and heterogeneous catalysis: A review on selected catalytic processes. *Catalysts* **2020**, *10*, 246. [CrossRef]
34. Zhan, H.; Shi, X.; Huang, X.; Zhao, N. Highly coke-resistant ordered mesoporous Ni/SiC with large surface areas in $CO_2$ reforming of $CH_4$. *J. Fuel Chem. Technol.* **2019**, *47*, 942–948. [CrossRef]

35. Liu, Z.; Zhou, J.; Cao, K.; Yang, W.; Gao, H.; Wang, Y.; Li, H. Highly dispersed nickel loaded on mesoporous silica: One-spot synthesis strategy and high performance as catalysts for methane reforming with carbon dioxide. *Appl. Catal. B Environ.* **2012**, *125*, 324–330. [CrossRef]
36. Tomiyama, S.; Takahashi, R.; Sato, S.; Sodesawa, T.; Yoshida, S. Preparation of Ni/$SiO_2$ catalyst with high thermal stability for $CO_2$-reforming of $CH_4$. *Appl. Catal. A Gen.* **2003**, *241*, 349–361. [CrossRef]
37. Ren, H.-P.; Hao, Q.-Q.; Wang, W.; Song, Y.-H.; Cheng, J.; Liu, Z.-W.; Liu, Z.-T.; Lu, J.; Hao, Z. High-performance Ni-$SiO_2$ for pressurized carbon dioxide reforming of methane. *Int. J. Hydrog. Energy* **2014**, *39*, 11592–11605. [CrossRef]
38. Rodríguez-González, V.; Marceau, E.; Beauniera, P.; Chea, M.; Train, C. Stabilization of hexagonal close-packed metallic nickel for alumina-supported systems prepared from Ni(II) glycinate. *J. Solid State Chem.* **2007**, *180*, 22–30. [CrossRef]
39. Ren, H.-P.; Hao, Q.-Q.; Ding, S.-Y.; Zhao, Y.-Z.; Zhu, M.; Tian, S.-P.; Ma, Q.; Song, W.-Q.; Miao, Z.; Liu, Z.-T. A high-performance Ni/$SiO_2$ prepared by the complexed-impregnation method with citric acid for carbon dioxide reforming of methane. *Ind. Eng. Chem. Res.* **2018**, *57*, 16257–16263. [CrossRef]
40. Zhang, Q.; Long, K.; Wang, J.; Zhang, T.; Song, Z.; Lin, Q. A novel promoting effect of chelating ligand on the dispersion of Ni species over Ni/SBA-15 catalyst for dry reforming of methane. *Int. J. Hydrog. Energy* **2017**, *42*, 14103–14114. [CrossRef]
41. Li, B.; Zhang, S. Methane reforming with $CO_2$ using nickel catalysts supported on yttria-doped SBA-15 mesoporous materials via sol-gel process. *Int. J. Hydrog. Energy* **2013**, *38*, 14250–14260. [CrossRef]
42. Jiang, N.; Xu, X.-W.; Song, H.-L.; Song, H.; Zhang, F.-Y. Effect of Citric Acid on the Hydrodesulfurization Performance of Unsupported Nickel Phosphide. *Ind. Eng. Chem. Res.* **2016**, *55*, 555–559. [CrossRef]
43. Castillo-Villalón, P.; Ramirez, J.; Vargas-Luciano, J.A. Analysis of the role of citric acid in the preparation of highly active HDS catalysts. *J. Catal.* **2014**, *320*, 127–136. [CrossRef]
44. Bian, Z.; Xin, Z.; Meng, X.; Tao, M.; Lv, Y.; Gu, J. Effect of citric acid on the synthesis of CO methanation catalysts with high activity and excellent stability. *Ind. Eng. Chem. Res.* **2017**, *56*, 2383–2392. [CrossRef]
45. Liu, D.; Quek, X.Y.; Cheo, W.N.E.; Lau, R.; Borgna, A.; Yang, Y. MCM-41 supported nickel-based bimetallic catalysts with superior stability during carbon dioxide reforming of methane: Effect of strong metal-support interaction. *J. Catal.* **2009**, *266*, 380–390. [CrossRef]
46. Shang, Z.; Li, S.; Li, L.; Liu, G.; Liang, X. Highly active and stable alumina supported nickel nanoparticle catalysts for dry reforming of methane. *Appl. Catal. B Environ.* **2017**, *201*, 302–309. [CrossRef]
47. Samojeden, B.; Kamienowska, M.; Colorado, A.I.; Galvez, M.E.; Kolebuk, I.; Motak, M.; Costa, P.D. Novel nickel- and magnesium-modified cenospheres as catalysts for dry reforming of methane at moderate temperatures. *Catalysts* **2019**, *9*, 1066. [CrossRef]
48. Zhang, C.; Zhu, W.; Li, S.; Wu, G.; Ma, X.; Wang, X.; Gong, J. Sintering-resistant Ni-based reforming catalysts obtained via the nanoconfinement effect. *Chem. Commun.* **2013**, *49*, 9383–9385. [CrossRef]
49. Zhang, Q.; Tang, T.; Wang, J.; Sun, M.; Wang, H.; Sun, H.; Ning, P. Facile template-free synthesis of Ni-$SiO_2$ catalyst with excellent sintering and coking-resistance for dry reforming of methane. *Catal. Commun.* **2019**, *131*, 105782. [CrossRef]
50. Wang, F.; Xu, L.; Shi, W. Syngas production from $CO_2$ reforming with methane over core-shell Ni@$SiO_2$ catalysts. *J. $CO_2$ Util.* **2016**, *16*, 318–327. [CrossRef]
51. Świrk, K.; Zhang, H.; Li, S.; Chen, Y.; Rønning, M.; Motak, M.; Grzybek, T.; Costa, P.D. Carbon-resistant NiO-$Y_2O_3$-nanostructured catalysts derived from double layered hydroxides for dry reforming of methane. *Catal. Today* **2020**. [CrossRef]
52. Charisiou, N.D.; Douvartzides, S.L.; Siakavelas, G.I.; Tzounis, L.; Sebastian, V.; Stolojan, V.; Hinder, S.J.; Baker, M.A.; Polychronopoulou, K.; Goula, M.A. The Relationship between Reaction Temperature and Carbon Deposition on Nickel Catalysts Based on $Al_2O_3$, $ZrO_2$ or $SiO_2$ Supports during the Biogas Dry Reforming Reaction. *Catalysts* **2019**, *9*, 676. [CrossRef]